Application of a Tubular Linear Actuator as an Axial Magnetic Bearing

Christoph Weißbacher, *Member, IEEE*, Hermann Stelzer, and Kay Hameyer, *Senior Member, IEEE*

***Abstract*—Magnetic bearing systems have been the subject of intense research for many years. In many applications, they have matured to state-of-the-art machine components. In this paper, the improvement and application of a previously introduced axial magnetic bearing is described. This bearing, a tubular linear actuator (TLA), does not only avoid some constructional problems, but also it combines positive axial stiffness with the possibility to actively influence axial bearing properties. Functionality and design of the TLA are described. The applicability as an axial bearing in a magnetic bearing system is shown, and force-displacement measurements are performed. The results are discussed, and the performance of the TLA as an axial magnetic bearing is evaluated.**

***Index Terms*—Magnetic levitation, system analysis and design.**

I. Introduction

DESIGN, performance, and application of magnetic bearing systems have been subject to numerous scientific publications. Most of these publications focus on radial magnetic bearings, while the design of axial magnetic bearings mostly remains unchanged, e.g., in [1]–[4]. In the usual design, a thrust disk is fixed on the rotor, as shown in Fig. 1.

The relatively large diameter of the thrust disk adds to some system design problems. Rotor unbalances are potentially larger. The maximum material strain increases because of the higher circumferential speed. In case of a rotor running in air, friction and noise level caused by air turbulences at the disk increase. Moreover, hermetic separation of rotor and stator by a closed air gap tube becomes significantly more difficult. This is especially important, because the separation possibility is one major advantage of magnetic bearing systems over conventional bearing systems, such as roller or plain bearings. With a magnetic bearing system, the rotor can run in vacuum or hazardous liquids or gases, while the bearings with their coils and cable connections are outside a closed container. In many applications of magnetic bearings, such as vacuum pumps or natural gas compressors, sealing is a major concern. Finally, mounting of the rotor-bearing system with a thrust disk becomes more complicated.

In [5], the axial bearing is implemented using the axial forces induced by the motor, avoiding a thrust disk for a very special rotor design that may not be an alternative in many applications. Another suggestion is made in [6], where reluctance forces are used to stabilize the rotor axially inside a closed container. However, there is no mechanism for controlling the axial position. Another possible alternative to the thrust disk concept is introduced in [7]. This bearing, a tubular linear actuator (TLA), does not employ a thrust disk. It is derived from a concept from the field of linear drives, e.g., as discussed in [8] and [9]. Relatively shallow grooves in the rotor, usually some millimeters deep, are used to exert axial forces on the rotor. The TLA is axially stable, but still enables position control in the axial direction, which can be used to actively influence bearing performance. However, the TLA is unstable in the radial direction. So whereas a thrust disk axial bearing does not alter radial bearing (RB) performance, the radial instability of the TLA has to be compensated.

The incorporation of a TLA, therefore, always is a tradeoff between radial and axial stiffnesses of the bearing system, and minimization of the negative radial stiffness is crucial.

The TLA introduced in [7] will subsequently be labeled TLA1. Some of its properties are shown in Table I.

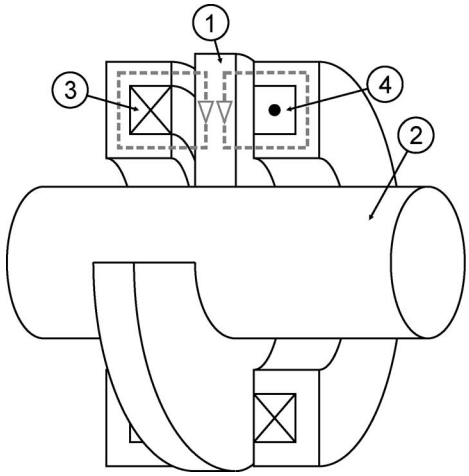

Fig. 1. Functional principle of a state-of-the-art thrust disk axial magnetic bearing. A thrust disk (1) is fixed upon a rotor (2). Coils (3) and (4) are used to modulate the air gap flux to cause the desired axial forces.

TABLE I
SOME PROPERTIES OF TLA1

Parameter	Value	
Maximum Load	900	N
Radial Stiffness (estimated)	-5000	N/mm
Rotor-Stator air gap	0.5	mm
Axial bearing height	65	mm
Outer diameter	186	mm
Inner diameter	75	mm

Manuscript received January 12, 2009; revised July 30, 2009; accepted August 9, 2009. Date of publication September 22, 2009; date of current version July 28, 2010. Recommended by Technical Editor W.-J. Kim.

C. Weißbacher and H. Stelzer are with the Department of Magnetic Bearings and Drives, Central Technology Division, Forschungszentrum Jülich GmbH, 52425 Jülich, Germany (e-mail: c.weissbacher@fz-juelich.de; h.stelzer@fz-juelich.de).

K. Hameyer is with the Institute for Electrical Machines, Rheinisch-Westfälische Technische Hochschule Aachen University, 52062 Aachen, Germany (e-mail: kay.hameyer@iem.rwth-aachen.de).

Digital Object Identifier 10.1109/TMECH.2009.2031111

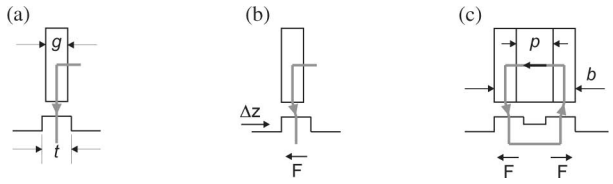

Fig. 2. (a) SRRP with dimensions t and g. (b) Axial restoring force and (c) TLA block setup with parameters p and b. The solid gray line indicates the magnetic flux.

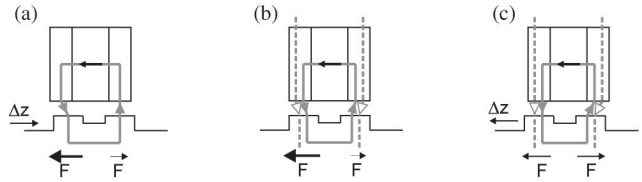

Fig. 3. (a) TLA force response to axial displacement and (b) EM flux (dashed gray line). (c) Application of the EM flux leads to a new axial position of force equilibrium.

Because of the very large negative radial stiffness, the attempt to include TLA1 into a magnetic bearing system was not successful. Ball bearings were used to stabilize the rotor radially in all tests on TLA1.

This paper takes the approach further. A TLA prototype with reduced negative radial stiffness is designed and implemented. It is incorporated into a magnetic bearing system and used to suspend a rotor magnetically in combination with two radial magnetic bearings. Radial and axial current-force-displacement characteristics of the TLA are measured, and a quantitative evaluation of the bearing performance is given.

II. Principle and Layout

A. Working Principle

The main functional parts of a TLA consist of ferromagnetic rotor teeth of width t and stator flux guidance rings of width g, with $t > g$. One of each is situated opposing each other. This combination constitutes a stator-rotor-ring pair (SRRP). A radial magnetic flux penetrates both parts of the SRRP. As shown in Fig. 2(a), as long as both rings are axially centered about each other, no force is exerted. As soon as one is dislocated in the axial direction, an axial restoring force F appears, see Fig. 2(b). Now two SRRPs and a permanent magnet (PM) with width p are combined to form a block with width $b = 2g + p$, as shown in Fig. 2(c). The opposing SRRPs are not centered, but the resulting axial forces cancel each other out if the rotor and stator blocks are axially centered.

In case of an axial displacement of the blocks, however, the force balance is disturbed and a total axial restoring force appears, as shown in Fig. 3(a). For control purposes, an electromagnetic (EM) flux can be applied to the setup, as shown in Fig. 3(b). The flux in the air gap of one SRRP of the block increases while the flux in the other air gap decreases, resulting in an axial force driving the rotor to a new point of force equilibrium, as shown in Fig. 3(c).

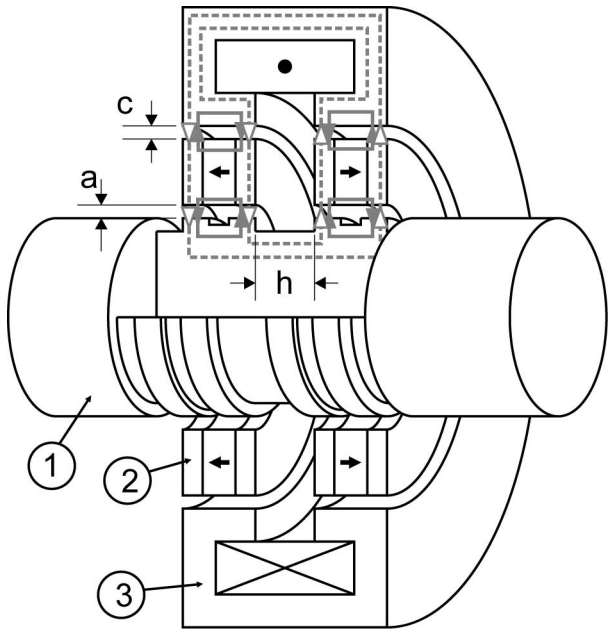

Fig. 4. Principal setup of a minimal TLA with the rotor (1), the PM part (2), and the EM part (3). Also shown are the air gaps a and c. The gray solid line symbolizes the PM, the gray dashed line the EM flux.

Resulting from the earlier considerations, the TLA geometry is stable in the axial direction and unstable in the radial direction, expressed by a positive axial and negative radial stiffnesses. In addition, the axial position can be controlled by application of a control flux. This property is expressed by the EM force current constant k_{EM} of the TLA.

B. TLA Components

A TLA is a magnetic bearing that consists mainly of three separate parts: the rotor, a PM part, and an EM part. Each of these has distinctive design parameters that add to the overall TLA performance. To simplify matters, a TLA with a minimum number of components is introduced here. The device can easily be expanded to increase system performance. All parts described in this section are shown in Fig. 4.

1) Rotor: As sketched in Fig. 2(c), the ferromagnetic rotor is equipped with two blocks of teeth that guide the flux. Each block consists of an even number n of teeth, and both blocks are identical. For the axial space between the blocks h, the relationship $h \gg 2(a + c)$ should be fulfilled to minimize stray flux.

No thrust disk is necessary, so its negative consequences are avoided. Hence, the rotor can easily be confined in a closed can of nonmagnetic material, e.g., carbon fiber composite material. This simplifies sealing of the rotor within the process chamber from the surroundings.

2) Permanent-Magnetic Part: To complete the geometry in Fig. 2(c), two blocks with each $n-1$ (with n being the number of teeth per block) PM rings and n ferromagnetic flux guidance rings are situated around the rotor. The PMs are axially polarized so that all adjacent rings as well as both blocks repel each other.

Thereby a maximum amount of permanent-magnetic flux closes via the rotor teeth.

This combination of rotor and PM part constitutes an axial magnetic bearing with rotor–stator air gap a. If the rotor is axially displaced from the shown center position, reluctance forces will counter the displacement, so the bearing has a positive axial stiffness. However, any radial displacement leads to radial forces that increase the displacement, arousing a negative radial stiffness.

3) Electromagnetic Part: To enable an EM flux as in Fig. 3(b), a control coil within a flux guidance housing is mounted around the PM part, constituting the stator permanent magnetic–electro magnetic (PM–EM) air gap c. This air gap has two influences: part of the PM flux closes via the coil housing, which reduces flux density in the rotor–stator air gap, causing reduced TLA stiffness for a small c. On the other hand, the EM flux also closes via this air gap, so a large c decreases the influence of the control coil.

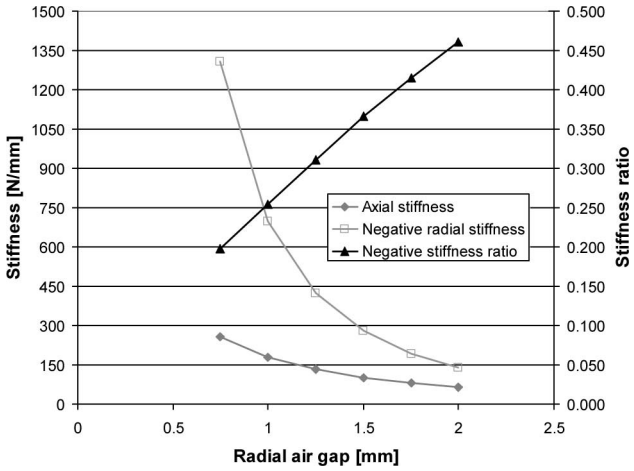

Fig. 5. Axial and radial stiffnesses and ratio of axial and negative radial stiffnesses for a double SRRP arrangement.

C. TLA Design and Implementation

A central aspect in TLA design is to find a layout that minimizes the radial instability while meeting the axial stiffness requirements and retaining an EM force current constant as large as possible. To find such a layout, a parametric study of the TLA is carried out. Because of the large air gaps and importance of edge effects, the complexity of an analytical model of the TLA is high. Hence, the TLA geometry is modeled using the finite-element method (FEM) simulation Tool *iMOOSE* [10]. For the axial characteristics, an axially symmetric 2-D FEM model is applied. The radial characteristics are calculated using a 3-D FEM model.

The designed TLA, subsequently called TLA2, should have similar geometric properties as TLA1 in Table I for good comparability. It should be able to passively support a rotor weight of at least 300 N with a maximum axial offset of 1.8 mm. The rotor diameter is given as 78 mm.

As design parameters, the rotor–stator air gap a, the PM–EM air gap c, flux guidance ring width g, and stator teeth width t are evaluated. The permanent magnet rings are given with an outer diameter of 100 mm, inner diameter of 81.5 mm, and axial height of 5 mm.

1) Influence of the Rotor–Stator Air Gap: For a first evaluation of the TLA characteristics depending on the rotor–stator air gap a, a double SRRP arrangement, as shown in Fig. 2(c), is analyzed. As seen in Fig. 5, the ratio of axial and negative radial stiffness significantly depends on this air gap.

The negative ratio of axial and radial stiffnesses increases approximately linearly with increasing air gap a. Therefore, the unwanted negative radial stiffness will for a maximum rotor–stator air gap be at a minimum. Since the PM ring inner diameter is fixed, the rotor–stator air gap is determined by the difference of rotor and PM ring radius. Leaving a security reserve of 0.05 mm for compensation of the mechanical tolerance of the permanent magnet rings, this gives a rotor–stator air gap of $a = 1.7$ mm.

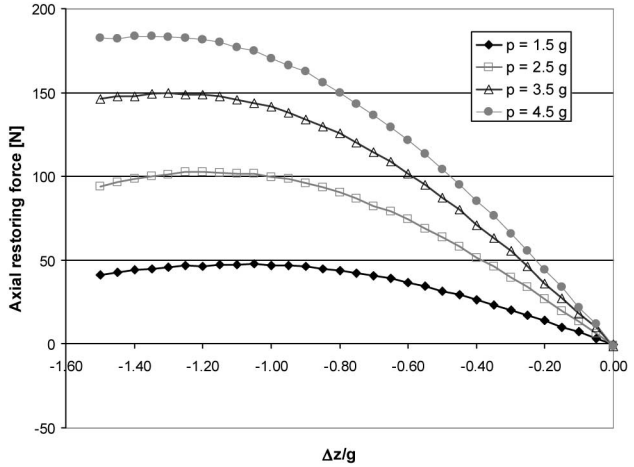

Fig. 6. Axial restoring force for a double SRRP arrangement.

2) Influence of the Guidance Ring Width: In Fig. 6, the axial force-displacement characteristics of a double SRRP arrangement, as shown in Fig. 2(c), are indicated.

The arrangement has a positive axial stiffness for at least $|\Delta z| < g$ for any ratio of p/g. Therefore, choosing a flux guidance ring height $g = 2.0$ mm will result in stable axial characteristics in the range $|\Delta z| < 2$ mm for TLA2. A number of four blocks of width $b = 9$ mm will result in a maximum force of around 400 N for the complete arrangement. This includes some force reserve for the expected reduction due to flux loss through the PM–EM air gap as explained in Section II-B3.

3) Influence of the PM–EM Air Gap c: Fig. 7 shows the influence of the ratio c/a on axial stiffness, and the EM force current constant k_{EM}.

As the ratio increases, a sixth-order polynomial approximation of the EM force current constant reaches a maximum at $c/a = 0.825$. For TLA2, the chosen value is $c/a = 0.88$, resulting in a PM–EM air gap of $c = 1.5$ mm.

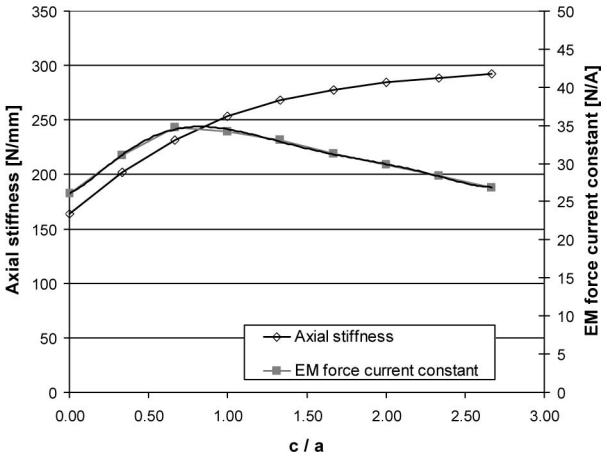

Fig. 7. Influence of the ratio *c*/*a* on axial stiffness and EM force current constant. A sixth-order polynomial approximation is overlaid the EM force current constant graph to indicate the position of the maximum.

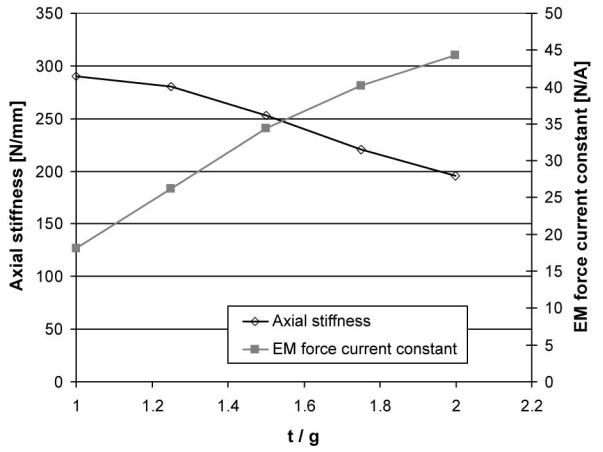

Fig. 8. Influence of the ratio *t*/*g* on axial stiffness and electromagnetic force current constant.

4) Influence of the Rotor Teeth Width t: In Fig. 8, the influence of the ratio *t*/*g* on axial stiffness and the EM force current constant k_{EM} is evaluated.

For an increasing ratio of *t*/*g*, the axial stiffness decreases, while the EM force current constant increases. However, the calculated axial stiffness refers to small axial displacements. As shown in Fig. 6, stiffness decreases significantly with increasing axial displacement. For linear force-displacement characteristics, the minimum axial stiffness would be 166.7 N/mm, resulting from the maximum rotor weight and the maximum axial displacement. To account for the nonlinearity, the chosen axial stiffness should be at least 50% larger, resulting in a minimum zero displacement stiffness of 250 N/mm. With Fig. 8, this results in a ratio of $t/g = 1.5$.

So for the earlier chosen values, a rotor teeth width of $t =$ 3 mm results.

Table II shows an overview of some design parameters of TLA2.

TABLE II
PROPERTIES OF TLA2

Parameter	Symbol	Value	
Rotor diameter	-	78	mm
TLA housing diameter	-	179	mm
TLA housing axial height	-	64	mm
Number of rotor teeth per block	n	4	
Rotor teeth width	t	3	mm
Rotor block width	b	9	mm
Rotor-stator air gap	a	1.7	mm
PM guidance ring width	g	2	mm
PM ring width	p	5	mm
Number of PM rings	$2n$-2	6	
Stator PM-EM air gap	c	1.5	mm
Maximum force at offset 1.8 mm	-	325	N
Number of windings	-	500	

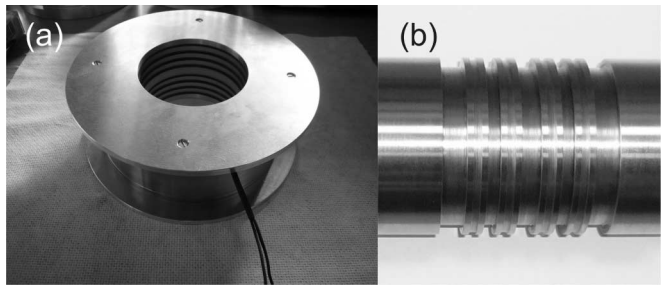

Fig. 9. Picture of the (a) implemented TLA before casting and (b) rotor.

Fig. 9 shows a picture of the implemented TLA2 stator and rotor parts. The rotor material is solid S235 steel. Since the TLA is a homopolar bearing, rotor iron and eddy current losses are expected to be relatively small. The flux guiding parts of the stator are made of solid C15 steel. For dynamic applications, lamination of the flux guiding parts is advisable.

For reasons of dimensional accuracy, voids in the TLA2 stator part are filled with a polyurethane cast resin after mounting. The complete device is then machined to the final dimensions to guarantee an accuracy of better than 50 μm for concentricity and inner and outer diameter of TLA2.

III. EXPERIMENTAL SETUP

A. Bearing System and Radial Force Measurement Setup

TLA2 is tested as a part of a complete magnetic bearing system. Two radial magnetic bearings are used to stabilize the rotor.

Prisms are used to mount the bearings on a machine bed, shown in Fig. 10. The mechanical setup of the RBs is such that one bearing is situated in the balance point of the rotor. This bearing therefore carries the whole rotor mass, while the other one balances the rotor. TLA2 is placed close to the load carrying bearing. Consequently, this RB can be used to measure the radial properties of TLA2 with the known load of the rotor weight of 193 N. Rotor displacement is available via the eddy-current sensors necessary for active radial control.

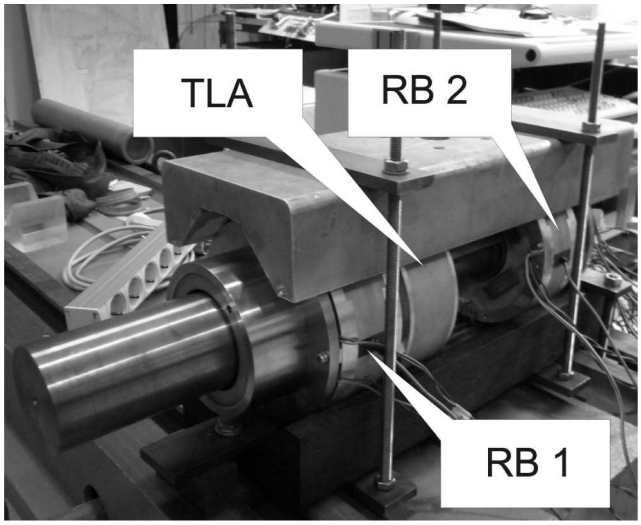

Fig. 10. Complete magnetic bearing system. The load-carrying RB1, the TLA, and the balancing RB2 are fixed on a machine bed.

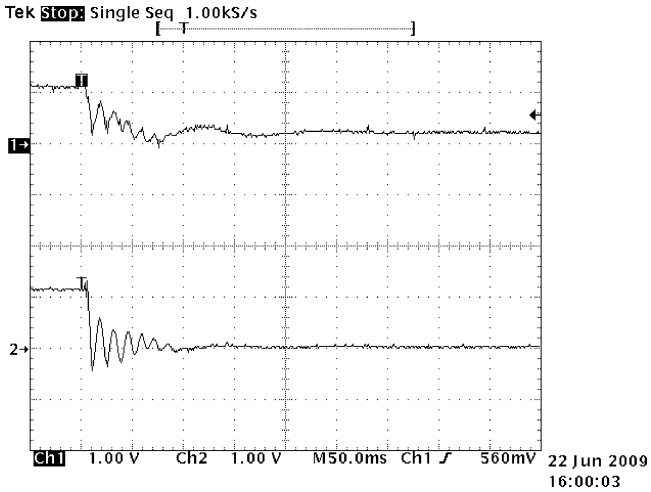

Fig. 11. Startup dynamics of the load carrying bearing (channel 1) and the balancing bearing (channel 2). The scale is 0.2 mm/V for both channels.

TABLE III
SYSTEM PARAMETERS OF THE RADIAL MAGNETIC BEARINGS

Parameter	Value	
Outer diameter	179	mm
Axial height	70	mm
Rotor-stator air gap	0.8	mm
Touchdown bearing air gap	0.2	mm
Maximum load	350	N
Maximum current	10	A
Supply Voltage	50	V

Table III shows some properties of the radial magnetic bearings.

Since the TLA adds a negative stiffness in the radial direction, the RBs will have to compensate this influence. In this application, the position sensors are placed within the RBs, and RB control is achieved with four separate digital PDI^2 controllers, implementing the transfer function

$$G(s) = v\frac{1 + s/s_n}{(1 + s/s_{p1})\,(1 + s/s_{p2})}.$$

The startup dynamics of the RBs are shown in Fig. 11.

B. Axial Force Measurement Setup

To measure the axial current-force-displacement characteristics, a piezoelectric force transducer is axially pressed against the levitating rotor. The displacement is measured using a state-of-the-art dial indicator. Fig. 12 shows a picture of the measurement setup.

Measurement inaccuracies are less than 1% for force and 10 μm for position measurement. The force transducer is not fixed to the rotor, so that levitation is still possible in the radial direction. Both RBs and TLA2 have a rotor–stator air gap large enough for an air gap tube of thickness 0.5 mm to be inserted. Such a tube may serve as a closed encapsulation between rotor and stator. If said tube is made of nonconductive material, as for example carbon fiber composite, state-of-the-art eddy-current sensors can be applied for rotor position measurement.

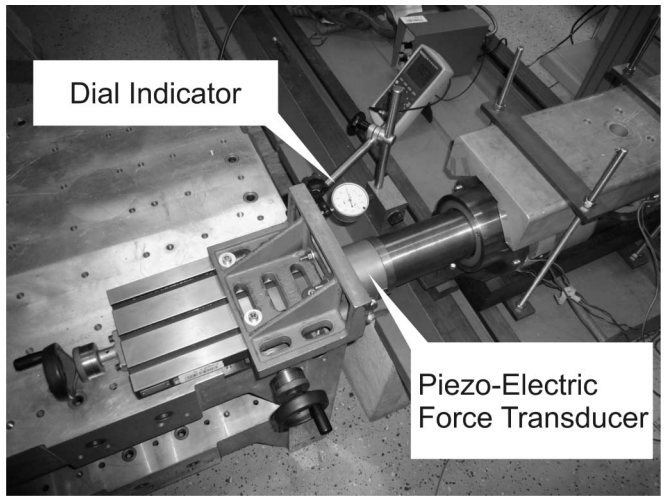

Fig. 12. Axial force measurement setup. A force transducer is pressed against the levitating rotor via a screw.

IV. MEASUREMENT RESULTS

A. Axial Characteristics

Since the TLA is symmetric in both axial directions, only one direction is measured. The measured current-force-displacement characteristics compared to the calculated characteristics are shown in Fig. 13.

A very good agreement between calculated and measured values can be seen. These characteristics are highly nonlinear, especially for large displacements. To evaluate the behavior of the axial stiffness caused by the permanent magnets as a function of displacement z, the measured characteristics at zero current

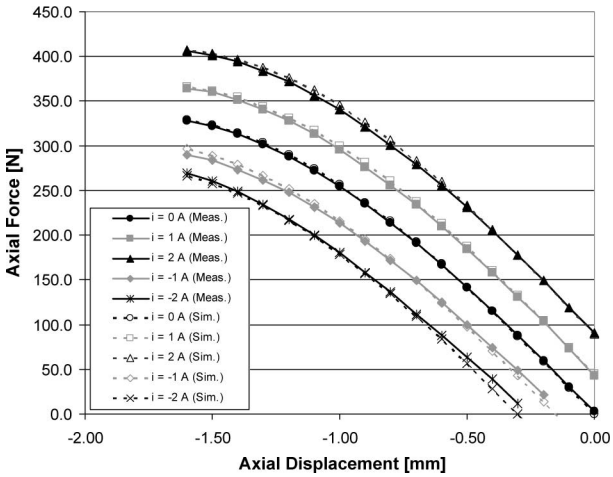

Fig. 13. Measured and calculated axial current-force-displacement characteristics of TLA2.

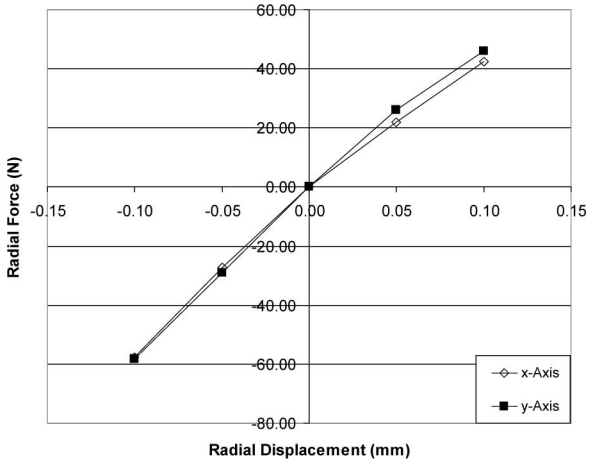

Fig. 14. Measured radial force-displacement characteristic of the TLA.

TABLE IV
COEFFICIENTS FOR THIRD-ORDER POLYNOMIAL APPROXIMATION OF THE AXIAL FORCE-DISPLACEMENT CHARACTERISTIC

Coefficient	Value	
k_3	25.821	N/mm³
k_2	-14.274	N/mm²
k_1	-292.69	N/mm
k_0	2.1655	N

are approximated as a third-order polynomial

$$F_{\mathrm{PM}}(z) = k_3 z^3 + k_2 z^2 + k_1 z + k_0 \tag{1}$$

with the coefficients, as shown in Table IV.

This approximation holds in the displacement range from 0 to -1.6 mm. The mse of the estimate in this range is 0.3%. The maximum of this function of 332.3 N is reached for an axial displacement of -1.768 mm. These values are in good agreement with the values in Table II.

Equivalently to the property of a mechanical spring, the differential axial stiffness is defined as

$$D_{\mathrm{PM}}(z) = -\frac{d}{dz} F_{\mathrm{PM}}(z). \tag{2}$$

Application of (2) on (1) yields the axial stiffness function

$$D_{\mathrm{PM}}(z) = -3k_3 z^2 - 2k_2 z - k_1 \tag{3}$$

for the aforementioned displacement range. The coefficient k_1 can be identified as the negative zero displacement axial stiffness.

In an application, linearization around the chosen bias point subsequently enables state-of-the-art position control, e.g., for damping or increasing dynamic stiffness.

Axial bearing forces caused by the control flux linearly superpose the forces caused by the displacement. Therefore, they can be accounted for by adding an extra term. The total axial measured current-force-displacement characteristics can consequently be summed up as

$$F_z(z, i) = F_{\mathrm{PM}}(z) + F_{\mathrm{EM}}(i) \tag{4}$$

with

$$F_{\mathrm{EM}}(i) = k_{\mathrm{EM}} i. \tag{5}$$

From the curves in Fig. 13, the EM force current constant can be deduced as

$$k_{\mathrm{EM}} = 43 \frac{N}{A}.$$

B. Radial Characteristics and Coupling

The radial measurement is performed in both control axes of the load-carrying RB. The rotor is via a current offset moved to the desired radial offset. The bearing currents are measured in both bearings, and from the known RB characteristics, the radial characteristics of the TLA are deduced.

Fig. 14 shows the measured radial force-displacement characteristic of the TLA.

As expected because of the circumferential homogeneity of the device, the radial force-displacement characteristics are nearly identical for both directions. The dependency of radial force on displacement is almost linear, with a negative radial stiffness of around -600 N/mm.

To evaluate the dynamic coupling between TLA and RBs, a sinusoidal current with a frequency of 6 Hz is applied to the TLA. Fig. 15 shows the results of this analysis.

For an applied current of amplitude 2 A, corresponding to an axial position amplitude of 0.3 mm, the radial deviations from the center position are merely 0.01 mm for RB1 and around 0.005 mm for RB2. Coupling between the TLA and the RBs is weak. Due to the symmetric structure and the permanent-magnetic excitation of the TLA, its radial stiffness does not largely depend upon axial position or applied current.

Resulting from the zero displacement stiffness and rotor mass, the TLA has a resonance frequency of around 19 Hz. Since no active control is implemented here, this resonance frequency is practically undamped.

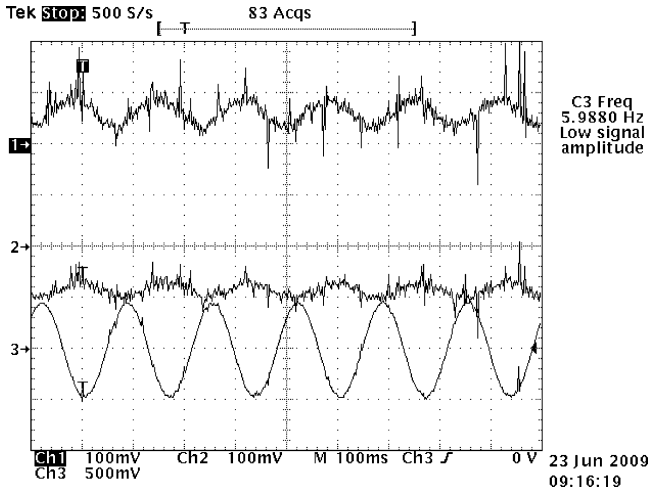

Fig. 15. Dynamic coupling between TLA and RBs. The reaction of RB1 (channel 1) and RB2 (channel 2) to a sinusoidal excitation of the TLA (channel 3) is evaluated. Scales are 0.2 mm/V for channels 1 and 2 and 4 A/V for channel 3.

TABLE V
COMPARISON OF THE PROPERTIES OF TLA1 AND TLA2

Property	TLA1	TLA2
Zero displacement axial stiffness [N/mm]	360	292.69
Axial EM force current constant [N/A]	86	43
Radial stiffness [N/mm]	-5000 (est.)	-600
Axial/Radial stiffness ratio	-0.072	-0.488
Maximum axial load [N]	900	325

C. TLA Characteristics Evaluation

Table V gives a comparison of the measured axial and radial characteristics of TLA1 and TLA2. Both bearings have very similar geometric dimensions. Therefore, a direct comparison between the two bearings gives a good impression of the effect of the adjustments made in the design process.

As the passive axial stiffness is similar, the EM force current constant of TLA2 is much lower. However, radial instability is also significantly reduced, enabling TLA2 to be applied as an axial magnetic bearing in the first place.

However, a certain amount of negative radial stiffness can advantageously be used for levitation of the rotor. To minimize power consumption of the bearing system, it is possible to suspend the rotor in a radial position where the forces exerted by gravity and the forces exerted by the permanent magnets cancel each other out. So the bearing system consumes very little electrical power at that bias point. The TLA can with its negative stiffness supply part of the compensation forces for minimum current operation.

V. CONCLUSION

The TLA introduced in this paper is an alternative to conventional axial bearings in magnetic bearing systems for completely encapsulated rotors, e.g., for pumps in aggressive media or in high vacuum. It enables a simple separating tube to be applied between rotor and stator that requires no additional sealings. All active bearing components can be situated outside the separation tube. The rotor can be balanced and mounted in one piece. A major source of rotor unbalances is removed from the system. However, these advantages are bought via reduced radial stiffness, which has to be compensated by the radial magnetic bearings.

Although the introduced improved TLA design may be better fit to application as an axial magnetic bearing, the improvement approach was an empiric one. Application of optimization algorithms for mechatronic actuators as in [11] may further improve and fully exploit the possibilities of this bearing type.

REFERENCES

[1] A. Kenny and A. B. Palazzolo, "Comparison of the dynamic response of radial and tangential magnetic flux thrust bearings," *IEEE/ASME Trans. Mechatronics*, vol. 7, no. 1, pp. 61–66, Mar. 2002.

[2] V. D. Bloodgood, Jr., N. J. Groom, and C. P. Britcher, "Further development of an optimal design approach applied to axial magnetic bearings," in *Proc. 7th Int. Symp. Magn. Bearings,* Zurich, Switzerland, Aug. 2000, pp. 489–494.

[3] M. D. Noh, S.-R. Cho, J.-H. Kyung, S.-K. Ro, and J.-K. Park, "Design and implementation of a fault-tolerant magnetic bearing system for turbomolecular vacuum pump," *IEEE/ASME Trans. Mechatronics*, vol. 10, no. 6, pp. 626–631, Dec. 2005.

[4] Z. Ren and L. S. Stephens, "Closed-loop performance of a six degree-of-freedom precision magnetic actuator," *IEEE/ASME Trans. Mechatronics*, vol. 10, no. 6, pp. 666–674, Dec. 2005.

[5] Y. Okada, N. Yamashiro, K. Ohmori, T. Masuzawa, T. Yamane, Y. Konishi, and S. Ueno, "Mixed flow artificial heart pump with axial self-bearing motor," *IEEE/ASME Trans. Mechatronics*, vol. 10, no. 6, pp. 658–665, Dec. 2005.

[6] P. Karutz, T. Nussbaumer, W. Gruber, and J. W. Kolar, "Novel magnetically levitated two-level motor," *IEEE/ASME Trans. Mechatronics*, vol. 13, no. 6, pp. 658–668, Dec. 2008.

[7] W.-L. Lee, W.-R. Canders, and W. Schumacher, "New approaches for axial magnetic bearings," in *Proc. 7th Int. Symp. Magn. Bearings,* Zurich, Switzerland, Aug. 2000, pp. 443–448.

[8] P.-E. Cavarec, H. B. Ahmed, and B. Multon, "New multi-rod linear actuator for direct drive, wide mechanical bandpass applications," *IEEE Trans. Ind. Appl.*, vol. 39, no. 4, pp. 961–970, Jul./Aug. 2003.

[9] L. E. Amraoui, F. Gillon, S. Vivier, P. Brochet, and M. Benrejeb, "Robust electromagnetic optimization of tubular linear actuators," *IEEE Trans. Magn.*, vol. 40, no. 2, pp. 1192–1195, Mar. 2004.

[10] D. van Riesen, C. Monzel, C. Kaehler, C. Schlensok, and G. Henneberger, "iMOOSE: An open-source environment for finite-element calculations," *IEEE Trans. Magn.*, vol. 40, no. 2, pp. 1390–1393, Mar. 2004.

[11] S. Behbahani and C. W. de Silva, "Mechatronic design quotient as the basis of a new multicriteria mechatronic design methodology," *IEEE/ASME Trans. Mechatronics*, vol. 12, no. 2, pp. 227–232, Apr. 2007.

Christoph Weißbacher (M'08) received the M.Sc. degree in electrical engineering from the Faculty of Electrical Engineering and Information Technology, Rheinisch-Westfälische Technische Hochschule (RWTH) Aachen University, Aachen, Germany, in 2006.

Since 2006, he has been a Researcher with the Institute of Electrical Machines, RWTH Aachen University. He is currently with the Magnetic Bearings and Drives Department, Forschungszentrum Jülich GmbH, Jülich, Germany. His research interests include the development of finite-element method codes for rotor dynamics as well as design and experimental testing of noncontact position sensors, radial and axial magnetic bearings, and complete magnetic bearing systems.

Hermann Stelzer received the M.Sc. degree in process systems engineering and the Ph.D. degree from Rheinisch-Westfälische Technische Hochschule Aachen University, Aachen, Germany.

He was a Computer-Aided Design Engineer, developing and operating finite-element method codes. In 1993, he was a Project Manager in the development of casks for the transport and disposal of spent fuel assemblies. Since 1999, he has been with the Forschungszentrum Jülich GmbH, Jülich, Germany. During the first three years at Jülich, he managed the assembly of large neutron scattering instruments. Since 2004, he has been the Head of the Department of Magnetic Bearing and Drives, Forschungszentrum Jülich GmbH. His current research interests include the development of permanent-magnetic bearing systems, the simulation of dynamical behavior and damping of fast rotating neutron and X-ray chopper discs and cylinders, as well as the development of other new applications for magnetic suspension systems.

Kay Hameyer (M'96–SM'99) received the M.Sc. degree in electrical engineering from the University of Hannover, Hannover, Germany, the Ph.D. degree from the University of Technology Berlin, Berlin, Germany, and the Habilitation degree in 2004 from Poznan University of Technology, Poznan, Poland.

He was with Robert Bosch GmbH, Stuttgart, Germany, as a Design Engineer for permanent-magnet servo motors and electrical energy supply system components. In 1988, he was a Member of the Staff, University of Technology Berlin. Until February 2004, he was a Full Professor of numerical field computations and electrical machines at the Katholieke Universiteit Leuven, Leuven, Belgium. He is currently a Full Professor and the Director of the Institute of Electrical Machines, and the Holder of the Chair "Electromagnetic Energy Conversion" at Rheinisch-Westfälische Technische Hochschule Aachen University, Aachen, Germany. His research interests include numerical field computation and simulation, design of electrical machines, particularly permanent-magnet excited machines and induction machines, and numerical optimization strategies.